PCCP

PAPER

Cite this: *Phys. Chem. Chem. Phys.*, 2018, **20**, 8848

Novel photocatalytic water splitting solar-to-hydrogen energy conversion: $CdLa_2S_4$ and $CdLa_2Se_4$ ternary semiconductor compounds

A. H. Reshak

Received 17th January 2018,
Accepted 19th February 2018

DOI: 10.1039/c8cp00373d

rsc.li/pccp

Comprehensive *ab initio* calculations from first- to second-principles methods are performed to investigate the suitability of non-centro-symmetric $CdLa_2S_4$ and $CdLa_2Se_4$ to be used as active photocatalysts under visible light illumination. The calculations reveal the direct band gap nature of both compounds with large absorption coefficients (10^4–10^5 cm^{-1}). The absorption edges of $CdLa_2S_4$ and $CdLa_2Se_4$ occur at λ = 579.3 nm and λ = 670.1 nm, and the optical band gaps are estimated to be 2.14 eV and 1.85 eV for $CdLa_2S_4$ and $CdLa_2Se_4$, respectively. These gaps are larger than 1.23 eV the required optical band gap for photocatalytic performance to split water under visible light illumination. The calculated potentials of the conduction band and the valence band edges indicate that $CdLa_2S_4$ and $CdLa_2Se_4$ have strong reducing powers for H_2 production. The obtained results reveal that the high photogenerated carrier mobility favors enhancement of the photocatalytic performance. It has been found that there is a large mobility difference between the electrons (e^-) and the holes (h^+), which is useful for the separation of e^- and h^+, reduction of e^- and h^+ recombination rate, and improvement of the photocatalytic activity. Based on these findings, one can conclude that $CdLa_2S_4$ and $CdLa_2Se_4$ satisfied all requirements to be efficient photocatalysts. This will greatly improve the search efficiency and greatly help experiments to save resources in the exploration of new photocatalysts with good photocatalytic performances.

1. Introduction

Hydrogen production *via* photocatalytic water splitting utilizing solar light has enormous potential in solving the global energy and environmental crisis. The requirements are to develop efficient photocatalysts which must satisfy some criteria such as high chemical and photochemical stability, effective charge separation and strong solar-light absorption. Photocatalytic water splitting is an efficient way to convert solar energy into clean H_2 energy. In order to utilize the solar energy efficiently, it is required that the photocatalysts should be sensitive to visible light, which makes up about 43% of the whole solar energy.[1] The other important requirement is that the photocatalysts must show efficient separation and migration abilities of the photoexcited carriers, due to the fact that the photocatalytic reaction utilizes the photoexcited electrons and holes migrating to the surface of the photocatalyst. The photocatalysis process doesn't produce any pollutants because it uses photon energy and water, and hence, it will make a great contribution to energy and environmental challenges in the near future. One good example of the photocatalyst is the ternary semiconductor compounds AB_mC_n (A = Cu, Ag, Zn, Cd,...; B = Al, Ga, In, La,... and C = S, Se, Te) with a chalcopyrite structure. These materials have attracted considerable attention in recent years due to their applications in optical sensing, light-emitting diodes, biological labeling, solar cells, and as photocatalysts.[2–13] The ternary semiconductor compounds with chalcopyrite structures with suitable band-edges can split water into hydrogen and oxygen stoichiometrically under visible light illumination. The sulfides, selenides and stable metals which contain elements with d^{10} electronic configurations (*i.e.*, Cd, Zn, and In) show good migration ability of the photoexcited carriers because their conduction bands are constructed from the hybridized and broadly dispersed sp orbitals. However, the surface of the materials comprise cadmium or mercury, which are toxic elements, is very sensitive with respect to Ar^+ ion-bombardment which causes significant changes in the element stoichiometry resulting in an abrupt decrease of Cd and Hg content in the top surface layers.[14] Therefore, the Cd and Hg content becomes free of Cd and Hg in the top surface layers. This treatment makes the top surface of the materials comprise free of Cd and Hg, and hence, free of risk which makes it possible to be used in advanced technological applications.[15–17]

New Technologies – Research Centre, University of West Bohemia, Univerzitni 8, 306 14 Pilsen, Czech Republic. E-mail: maalidph@yahoo.co.uk; Fax: +420-386 361255; Tel: +420-777729583

We would like to highlight that Guangjian *et al.*[6] and Zhu *et al.*[13] reported the photocatalytic properties of $CdLa_2S_4$. To the best of our knowledge, no comprehensive work neither experimental data on the transport and optical properties nor first principles calculations on the structural, electronic, transport, photocatalytic and optical properties of $CdLa_2X_4$ (X = S or Se) have appeared in the literature. Therefore, as a natural extension to previous existing work detailed depiction of the electronic structure, transport, photocatalytic and optical properties of $CdLa_2X_4$ (X = S or Se) using a full potential method is timely and would bring us important insights in understanding the origin of the band structure, density of states, photocatalytic and photophysical properties. Hence, it is very important to use a full potential method based on the density functional theory (DFT). The full-potential method[18] within different types of exchange correlation (XC) potentials, namely general gradient approximation (PBE-GGA)[19] and modified Becke–Johnson potential (mBJ),[20] are used to ascertain the influence of the XC on the resulting band gap, and hence, on the photocatalytic properties of $CdLa_2X_4$ (X = S or Se). In this work, *ab initio* calculations from first- to second-principles methods are performed to investigate the suitability of the non-centro-symmetric $CdLa_2X_4$ (X = S or Se) to be used as active photocatalysts under visible light irradiation.

In this work *ab initio* calculations from first- to second-principles methods[18,21–24] are performed to investigate the suitability of $CdLa_2S_4$ and $CdLa_2Se_4$ to be used as active photocatalysts under visible light illumination. In recent years, due to the improvement of computational technologies, it has been proven that first-principles calculations are a strong and useful tool to predict the crystal structure and properties related to the electron configuration of a material before its synthesis.[25–33] It is well known that DFT approaches have the ability to accurately predict the ground state properties of the materials, and the developed analysis tools are vital for investigating their intrinsic mechanism. This microscopic understanding has further guided the molecular engineering design for new crystals with novel structures and properties. It is anticipated that first-principle material approaches will greatly improve the search efficiency and greatly help experiments to save resources in the exploration of new materials with good performances.[25–33] For instance, several researchers have used DFT calculations to explore new photocatalysts and they have found good agreement with the experimental results.[34–40]

We would like to mention that, in our previous works,[41–44] we have calculated the photocatalytic properties and the energy band gaps using a full potential method for several systems whose photocatalytic and energy band gaps are known experimentally and a very good agreement with the experimental data was obtained. Thus, we believe that our calculations reported in this paper would produce very accurate and reliable results which will greatly help experiments to save resources in the exploration of new photocatalysts with good photocatalytic performances. The aim of this work is to focus on the photocatalytic activity of non-centro-symmetric $CdLa_2S_4$ and $CdLa_2Se_4$ as new, green and efficient photocatalysts.

2. Methodology aspect

In this study, two types of ternary semiconductor compounds with non-centro-symmetric chalcopyrite structures are investigated for their suitability to be used as active photocatalysts in the visible light region. The two compounds are $CdLa_2S_4$ and $CdLa_2Se_4$ with tetragonal symmetry ($I\bar{4}2d$) and lattice parameters $a = b = 8.5919900$ Å, $c = 9.00872271$ Å and $Z = 4$ for $CdLa_2S_4$,[45] and $a = b = 8.93262736$ Å, $c = 9.40390262$ Å and $Z = 4$ for $CdLa_2Se_4$.[46] The crystal structure of $CdLa_2S_4$ and $CdLa_2Se_4$ form through a combination of the covalent CdX_4 and LaX_8 structural units (Fig. 1). The X-ray diffraction data[45,46] are used as an input to calculate the ground state properties of $CdLa_2S_4$ and $CdLa_2Se_4$. As the first step, the reported lattice constants and the atomic positions[45,46] are optimized using the full-potential method (wien2k package[18]) within the generalized gradient approximation (PBE-GGA)[19] as shown in Tables 1 and 2. The resulting relaxed geometrical structures are used to calculate the ground state properties, and hence, the photocatalytic properties of $CdLa_2S_4$ and $CdLa_2Se_4$ utilizing the recently modified Becke–Johnson potential (mBJ).[20] To achieve accurate results the muffin-tin spheres (R_{MT}) are chosen in such a way that the spheres did not overlap. Therefore, to insure that no charge leakage is left out of the atomic sphere cores the $R_{MT's}$ are chosen to be 2.5 atomic unit (a.u.) for Cd, La, and Se while it is 2.31 a.u. for S. We should emphasize that to achieve the total energy convergence the basis functions in the interstitial region (IR) are expanded up to $R_{MT} \times K_{max} = 7.0$ and inside the atomic spheres for the wave function, the l_{max} is taken to be equal to 10, and the charge density is Fourier expanded up to $G_{max} = 12$ (a.u.)$^{-1}$. A mesh of 1000 $\vec{k}$ points in the irreducible Brillouin zone (IBZ) is used to obtain the self-consistency which is converged since the total energy of the system is stable within 0.01 mRy. The ground state properties, and hence the photocatalytic properties are obtained using 50 000 $\vec{k}$ points in the IBZ. The modified tetrahedron method[47] is used to calculate the total and partial density of states (DOS). The inputs required for DOS calculations are the energy eigenvalues and eigenfunctions which are the natural outputs of band structure calculations.

3. Results and discussion

3.1. Photo-electrochemical properties

For photocatalytic performance under visible light illumination, it is necessary to have a material with an optical band gap larger than 1.23 eV in order to split the water.[48] For use in photocatalytic water splitting, the optical band gap of the photocatalyst material must be sufficiently large to overcome the endothermic character of the water-splitting reaction, *i.e.* larger than 1.23 eV. Moreover, the positions of the conduction band minimum (CBM) and the valence band maximum (VBM) are very crucial requirements in photocatalytic water splitting. For instance, the CBM must be more negative than the reduction potential of H^+ to H_2 (E_{H^+/H_2} = 0.0 V *vs.* NHE at pH = 0.0), and the VBM must be more positive than the oxidation potential of water (E_{O_2/H_2O} = 1.23 V *vs.* NHE at pH = 0.0) in order to evolve oxygen (Fig. 1b). Which implies that

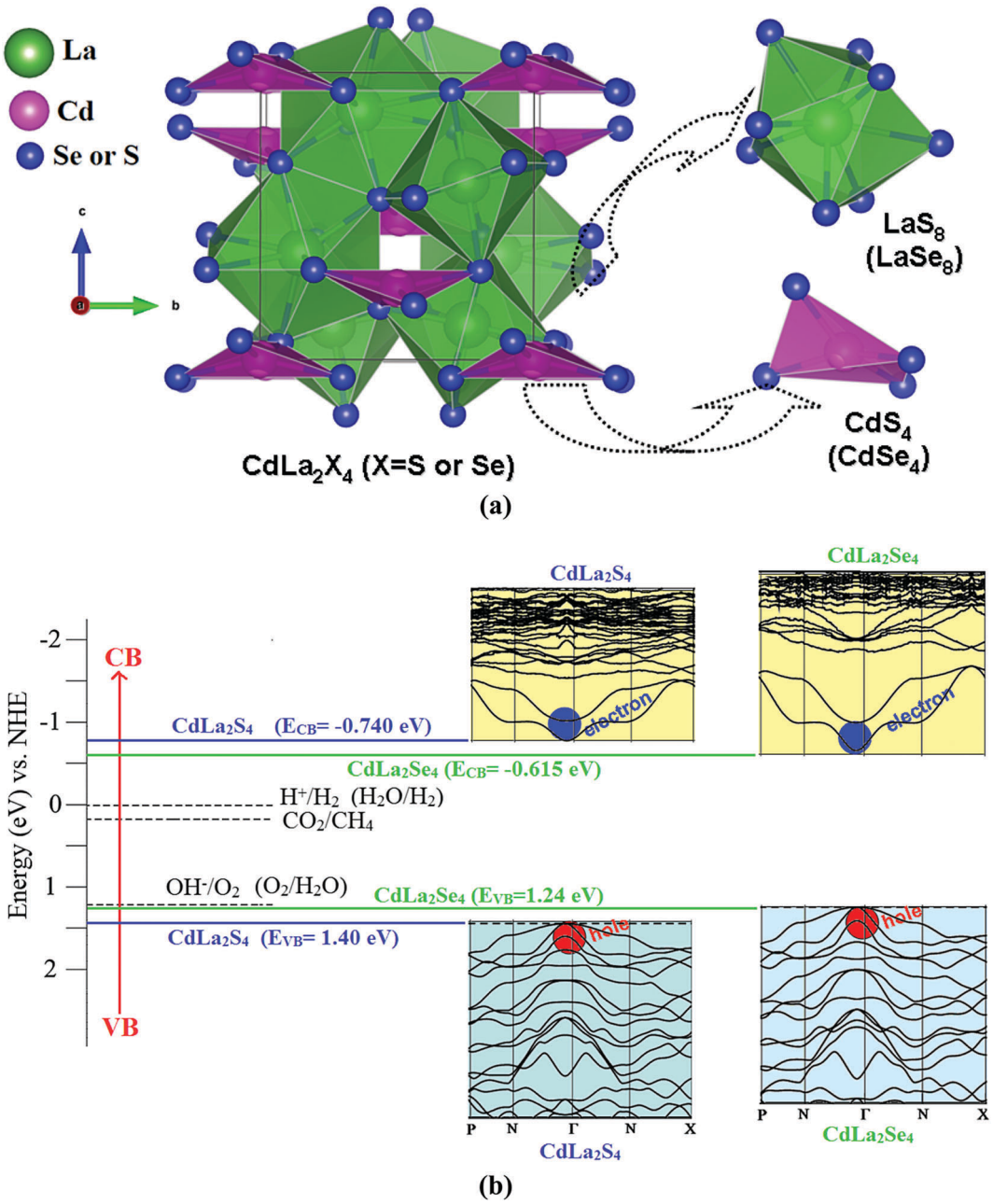

Fig. 1 (a) Crystal structure of $CdLa_2S_4$ and $CdLa_2Se_4$ with tetragonal symmetry ($I\bar{4}2d$) and lattice parameters $a = b = 8.5919900$ Å, $c = 9.00872271$ Å and $Z = 4$ for $CdLa_2S_4$, and $a = b = 8.93262736$ Å, $c = 9.40390262$ Å and $Z = 4$ for $CdLa_2Se_4$. The crystal structure of $CdLa_2S_4$ and $CdLa_2Se_4$ forms through a combination of the covalent CdX_4 and LaX_8 structural units; (b) the E_{CB} and E_{VB} values of $CdLa_2S_4$ and $CdLa_2Se_4$.

the photocatalytic activities are directly related to the materials electronic band structure.[49] Therefore, we investigated the electronic band structure of $CdLa_2S_4$ and $CdLa_2Se_4$ as shown in Fig. 2a and b. The calculated electronic band structures explore the positions of the VBM, CBM, the value and the nature of the fundamental energy band gaps. Fig. 2a and b reveals the direct band gap nature of $CdLa_2S_4$ and $CdLa_2Se_4$ since the valence VBM and the CBM are located at Γ point of the BZ, which implies that the electrons (e^-) can recombine directly with holes (h^+).

Both $CdLa_2S_4$ and $CdLa_2Se_4$ crystallize in a non-centro-symmetric structure; it is interesting to highlight that the non-centro-symmetric structure induces a spontaneous polarization due to the displacement of the center of the positive and negative charges in a unit cell.[50] As their positive and negative charges have different centers of symmetry, the non-centro-symmetric materials belong to ferroelectric materials that have a macroscopic polarization which induces the accumulation of charges at the surfaces.[51] Thus, a spontaneous polarization can be screened by free electrons in the CB and free holes in the VB, and/or by ions adsorbed on the surface from the solution forming a Stern layer.[52] A positive charge in positive fields is screened by external and internal mechanisms.[53] The internal

Table 1 Optimized lattice constants and the atomic positions of $CdLa_2S_4$ in comparison with the available data[45]

Cell parameters (Å)		$a = b$		c	
Ref. 20		8.5919900		9.00872271	
This work		8.5918988		9.0079877	
Atomic positions					
Atom	x^a	x optim.	y^a	y optim.	z^a	z optim.
Cd	0.000000	0.000000	0.000000	0.000000	0.000000	0.000000
La	0.142454	0.142399	0.250000	0.250000	0.625000	0.624000
S	0.068753	0.068698	0.197081	0.196911	0.312699	0.312678

[a] Ref. 45.

Table 2 Optimized lattice constants and the atomic positions of $CdLa_2Se_4$ in comparison with the available data[46]

Cell parameters (Å)		$a = b$		c	
Ref. 21		8.93262736		9.40390262	
This work		8.93219855		9.40389201	
Atomic positions					
Atom	x^a	x optim.	y^a	y optim.	z^a	z optim.
Cd	0.000000	0.000000	0.000000	0.000000	0.000000	0.000000
La	0.138043	0.137935	0.250000	0.250000	0.125000	0.124000
Se	0.069394	0.068432	0.194870	0.194669	0.810563	0.810323

[a] Ref. 46.

mechanism forms a negatively charged region below the surface, and the external mechanism consists of the adsorption of foreign negatively charged ions at the surface, whereas the opposite reactions take place in negative fields, and the adsorbed foreign ions are positively charged. This charge reallocation generates an electric field around the charge region.[54] A polarization field is compensated at equilibrium by the screening mechanisms. Thus, the photogenerated electrons can easily migrate to the surface and give rise to oxidation and reduction products at different locations.[55] This in turn enhances the photocatalytic activity. We should emphasize that the unique photochemistry of the non-centro symmetric materials may be utilized to launch some new photoreaction pathways. It is well known that CdX_4 is one of the most active groups in non-centro symmetric crystals and possesses a polarized covalent bonding. Moreover, the Cd–X units possess a strong electron cloud overlap and prefer to attract h^+ and repel e^-, thus facilitating separation of the photogenerated e^-–h^+ pairs. This in turn enhances the photocatalytic activity. It is interesting to highlight that the polarizability results in lowering of the potential energy of the charged particles and transition states regardless of whether these particles are negatively or positively charged.[56]

The photocatalytic oxidation of the materials is mainly attributed to the participation of superoxide radicals ($O_2^{\bullet -}$), hydroxyl radicals ($^\bullet$OH) and photogenerated holes,[57] see Fig. 2c. In order to understand the photocatalytic mechanism of $CdLa_2S_4$ and $CdLa_2Se_4$, the reduction and oxidation potentials of CB and the VB edges at the point of zero charge can be calculated following the expressions given in ref. 58:

$$E_{CB} = \chi - E^C - (E_g/2) \quad (1)$$

$$E_{VB} = E_{CB} + E_g \quad (2)$$

where E_{CB} and E_{VB}, respectively, are the potentials of the conduction band and valence band edges, E^C is the free energy corresponding to the hydrogen scale, and the value is ~4.5 eV,[58] E_g and χ are the band gap and the electronegativity of semiconductors, respectively. The χ is defined as the geometric mean of the absolute electronegativities of the constituent atoms. The absolute electronegativity of an individual atom is the arithmetic mean of the atomic electron affinity and the first ionization energy.[58] The E_{CB} and E_{VB} values of $CdLa_2S_4$ and $CdLa_2Se_4$ are shown in Table 3 and Fig. 1b. This figure illustrates the probable energy level diagram (potential *vs.* NHE) and CO_2 photoreduction, displaying the relative positions of CB and VB for $CdLa_2S_4$ and $CdLa_2Se_4$, and redox potentials for CO_2/CH_4 and O_2/H_2O. $CdLa_2Se_4$ appears as a more efficient photocatalyst for CO_2 photoreduction, possessing a CBM at −0.615 eV, and a corresponding VBM at 1.24 eV. The downward shifted CB bottom lies above the redox potential of CO_2/CH_4 (0.17 eV), whereas the VB top lies above the O_2/H_2O redox potential (1.23 eV).[59] It can be clearly seen that the CB edge potential of $CdLa_2S_4$ is more negative than that of $CdLa_2Se_4$, indicating that $CdLa_2S_4$ has a stronger reducing power for H_2 production than $CdLa_2Se_4$. A semiconductor with a more negative CB edge potential has a stronger reducing power for the H_2 production from water.[58] It can be clearly seen that the CB edge potential becomes more negative with increasing optical band gap and with substitution of Se by S. Generally, an appropriate band gap width and suitable CB edge position together attribute to the optimal H_2 production activity under light irradiation. Therefore, a balance between the light absorption capacity and the reducing power in the investigated materials leads to a higher efficiency of light-driven photocatalytic H_2 production.

The other crucial issue in the photocatalytic activities is the size of the optical band gap, therefore, we have calculated the absorption spectrum of $CdLa_2S_4$ and $CdLa_2Se_4$ as shown in Fig. 2d and e to estimate the size of the optical band gap. It is clear that the direct band gap semiconductors have large absorption coefficients (10^4 cm^{-1}). The optical band gap value of the semiconductor materials could be solved as follows; the square of absorption coefficient $I(\omega)$ is linear with energy (E) for direct optical transitions in the absorption edge region, whereas $\sqrt{I(\omega)}$ is linear with E for indirect optical transitions.[60,61] Since the calculated electronic band structure of $CdLa_2S_4$ and $CdLa_2Se_4$ confirms the direct nature of the band gap therefore, the data plots of $[I(\omega)]^2$ *vs.* E show the linear relationship between $[I(\omega)]^2$ and E in the absorption edge region, as shown in Fig. 2f and g. These plots suggest that the absorption edge of $CdLa_2S_4$ and $CdLa_2Se_4$ is caused by direct transitions. Following Fig. 2f and g, we can conclude that the absorption edges of $CdLa_2S_4$ and $CdLa_2Se_4$ occur at λ = 579.3 nm and λ = 670.1 nm, and the optical band gaps are estimated ($\lambda_g = 1239.8/E_{g(optical)}$[62]) to be 2.14 eV and 1.85 eV for $CdLa_2S_4$ and $CdLa_2Se_4$, respectively.

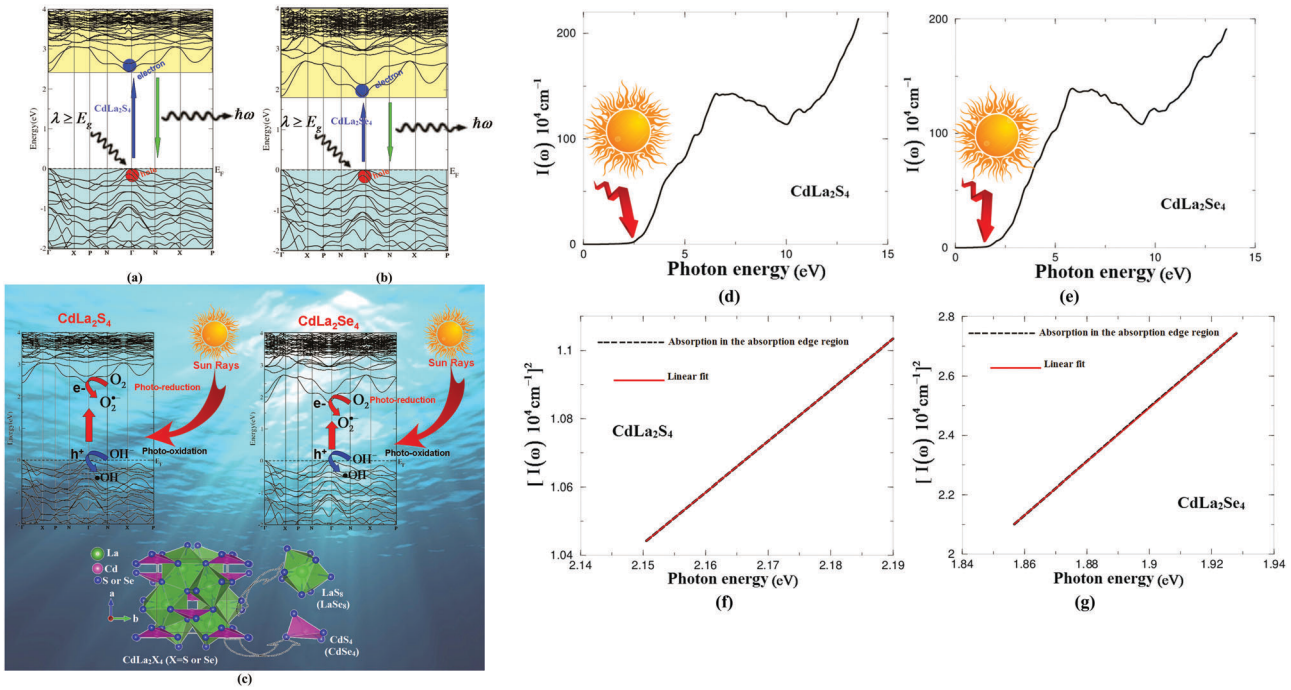

Fig. 2 (a and b) The calculated electronic band structure which clearly show the conduction band minimum, valence band maximum and the energy band gap; (c) schematic diagrams of charge transfer and photocatalytic mechanism of $CdLa_2S_4$ and $CdLa_2Se_4$; when a photocatalyst absorbs radiation from sunlight, it produces electron and hole pairs. The electron of the valence band becomes excited when illuminated by light. The excess energy of this excited electron promoted the electron to the conduction band therefore, creating the negative electron (e^-) and positive hole (h^+) pair. This stage is referred to as the semiconductor's 'photo-excitation' state; (d and e) calculated absorption coefficient of $CdLa_2S_4$ and $CdLa_2Se_4$ it is clear that the direct band gap semiconductors have large absorption coefficients (10^4–10^5 cm^{-1}); (f and g) the estimated optical band gap values of $CdLa_2S_4$ and $CdLa_2Se_4$, the data plots clearly show that $[I(\omega)]^2$ *versus* E is linear in the absorption edge region thus, the absorption edge of $CdLa_2S_4$ and $CdLa_2Se_4$ is caused by direct transitions. The absorption edges of $CdLa_2S_4$ and $CdLa_2Se_4$ occur at λ = 579.3 nm, and λ = 670.1 nm, and the optical band gaps are estimated to be 2.14 eV, and 1.85 eV for $CdLa_2S_4$ and $CdLa_2Se_4$, respectively.

Table 3 The calculated E_{CB} and E_{VB}

Compound	E_{CB} (eV)	E_{VB} (eV)
$CdLa_2S_4$	−0.740	1.40
$CdLa_2Se_4$	−0.615	1.24

The obtained band gaps show good agreement with the available experimental data[6,13] and are much better than the reported values using VASP code within GGA,[45,46] due to the fact that GGA underestimates the energy band gap value.[63] While the mBJ is a modified Becke–Johnson potential, which allows calculation of the energy band gap with an accuracy similar to that of the very expensive GW calculations.[20] It is a local approximation to an atomic "exact-exchange" potential and a screening term. Therefore, based on our experience in using different XC functionals (LDA, PBE-GGA, EV-GGA, LDA-mBJ and PBE-GGA-mBJ) on several systems whose energy band gaps are known experimentally,[63–65] in those previous calculations we found that the PBE-GGA-mBJ gives very good agreement with the experimental data.[64–66] This motivated us to use PBE-GGA-mBJ to calculate the band structure, and hence, the related properties of $CdLa_2S_4$ and $CdLa_2Se_4$.

The other crucial issues to understand the photocatalytic mechanisms in $CdLa_2S_4$ and $CdLa_2Se_4$, are the carriers concentration (n) and their mobility. Therefore, we have investigated the influence of temperature (T) on the carrier concentration (n) of $CdLa_2S_4$ and $CdLa_2Se_4$ at a certain value of chemical potential ($\mu = E_F$). It is clear that the carrier concentration of both compounds (Fig. 3a) shows a slight deviation from the linear temperature dependence and the positive sign indicates that $CdLa_2S_4$ and $CdLa_2Se_4$ exhibit p-type conductions. It has been noticed that the carrier concentration of $CdLa_2S_4$ is slightly higher than that of $CdLa_2Se_4$. To support this statement, we have investigated the n in the vicinity of E_F at three T values, as shown in Fig. 3b and c. It has been noticed that the difference between chemical potential and Fermi energy ($\mu - E_F$) is positive for valence bands and negative for conduction bands and $CdLa_2S_4$ and $CdLa_2Se_4$ exhibit a maximal n in the vicinity of E_F.

For an efficient photocatalytic mechanism, a material with the high mobility carriers is required. To achieve this, a material with small effective masses is needed. It has been noticed from the electronic band structure (Fig. 2a and b) that the high k-dispersion bands around the Fermi level (E_F) possess low effective masses and, hence, the high mobility carriers (Table 4) which favor an enhancement of the charge transfer process, and that the effective mass provides essential information regarding the photocatalytic mechanism. The mobility of the photogenerated carriers significantly influences the photocatalytic efficiency[67,68] and the higher photogenerated carrier mobility enhances the photocatalytic performance.[69–73] Moreover, the great

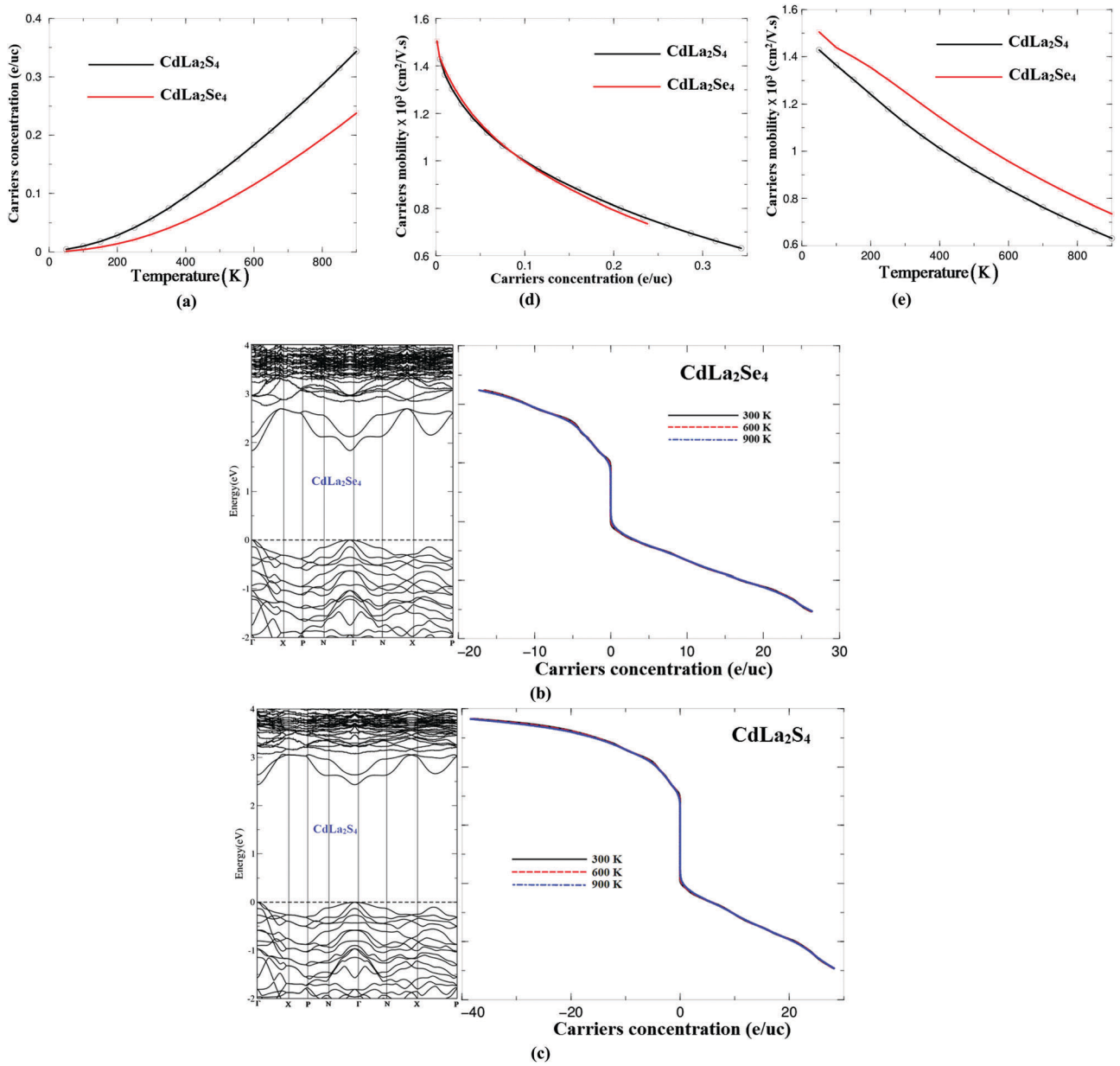

Fig. 3 (a) The carrier concentration of $CdLa_2S_4$ and $CdLa_2Se_4$ as function of temperature; (b and c) the carrier concentration of $CdLa_2S_4$ and $CdLa_2Se_4$ as function of chemical potential $\mu - E_F$ at room temperature and two other randomly selected temperatures; (d) the mobility of $CdLa_2S_4$ and $CdLa_2Se_4$ as a function of carrier concentration; (e) the mobility of $CdLa_2S_4$ and $CdLa_2Se_4$ as a function of temperature.

Table 4 Calculated effective masses

Effective mass	$CdLa_2S_4$	$CdLa_2Se_4$
m_e^*/m_o	0.01303	0.00695
m_{hh}^*/m_o	0.08479	0.05930
m_{lh}^*/m_o	0.01023	0.00799
$D = m_{hh}^*/m_e^*$	6.50729	8.53237
$D = m_e^*/m_{hh}^*$	0.15367	0.11720
$D = m_{lh}^*/m_e^*$	0.78511	1.14964
$D = m_e^*/m_{lh}^*$	1.27370	0.86983

effective mass difference ($D = m_h^*/m_e^*$ and $D = m_e^*/m_h^*$) between electron (e^-) and hole (h^+) (Table 4) can facilitate the e^- and h^+ migration and separation, and finally improve the photocatalytic performance.[70–73] The effective mass of e^- is bigger than that of h^+, resulting in a significant difference in the mobility between e^- and h^+. Therefore, the mobility of e^- is much higher than that of h^+, which consequently results in a striking difference in the mobility between the photoexcited e^- and h^+. This character is beneficial in suppressing the recombination of the e^-–h^+ pairs and improving the photocatalytic efficiency.[70–73] The mobility of photoexcited carriers can be indirectly assessed by their effective mass ($\eta_e = e\tau_e/m_e^*$ and $\eta_h = e\tau_h/m_h^*$); here we call the mobility η in order to distinguish between the mobility and chemical potential (μ). The large mobility difference is useful in the separation of e^- and h^+, in the reduction of the e^- and h^+ recombination rate,

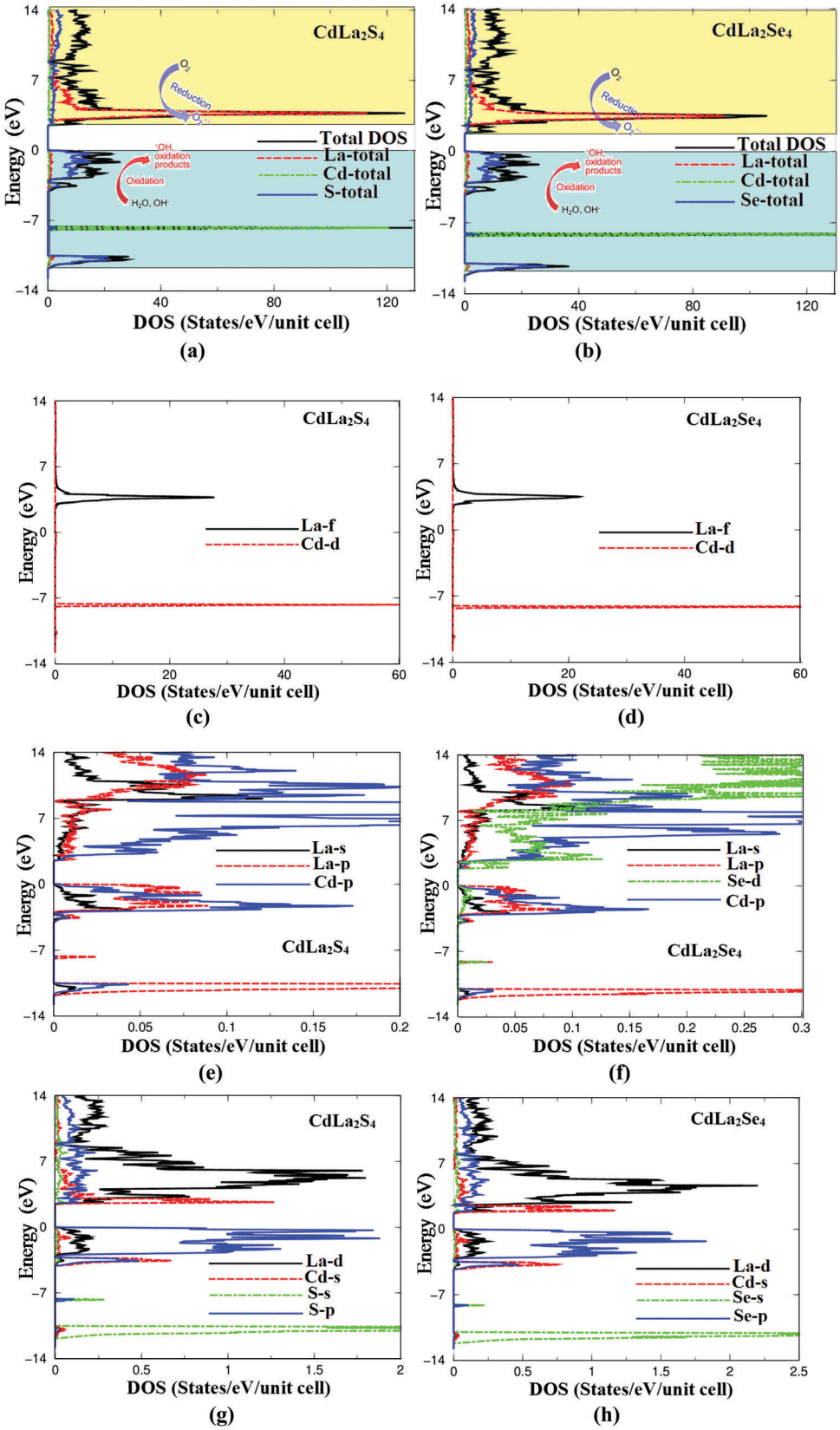

Fig. 4 (a–h) The projected density of states along with the angular momentum character of various structures for of $CdLa_2S_4$ and $CdLa_2Se_4$.

and in the improvement of the photocatalytic activity. It is clear from Table 4, that the effective mass of e^- and h^+ are small, and thus, we can deduce that the photogenerated carrier transfer can be fast along different directions. Fig. 3d shows the carrier mobility as a function of carriers concentration (n) which clearly shows a significant reduction in the carrier mobility by increasing the carriers concentration due to increasing the scattering. To support this statement we have investigated the carrier mobility as a function of temperature as shown in Fig. 3e. A significant reduction in the carrier mobility with increasing temperature is clearly shown which is attributed to the fact that raising the temperature causes an increase in the vibration, and hence, the mobility resulting in an increase in the scattering which leads to suppression of the mobility.

3.2. Structure–property and electronic charge density relationship

To gain a deeper insight into the photocatalytic mechanism in $CdLa_2S_4$ and $CdLa_2Se_4$, the angular momentum projected density of states are investigated as shown in Fig. 4a–h. The electronic band structure of both compounds shows highly dispersive CB and VB which provide favorable support to facilitate the transport of photoinduced charge carriers, which is considered to be a significant process for photocatalysis. Furthermore, it shows the

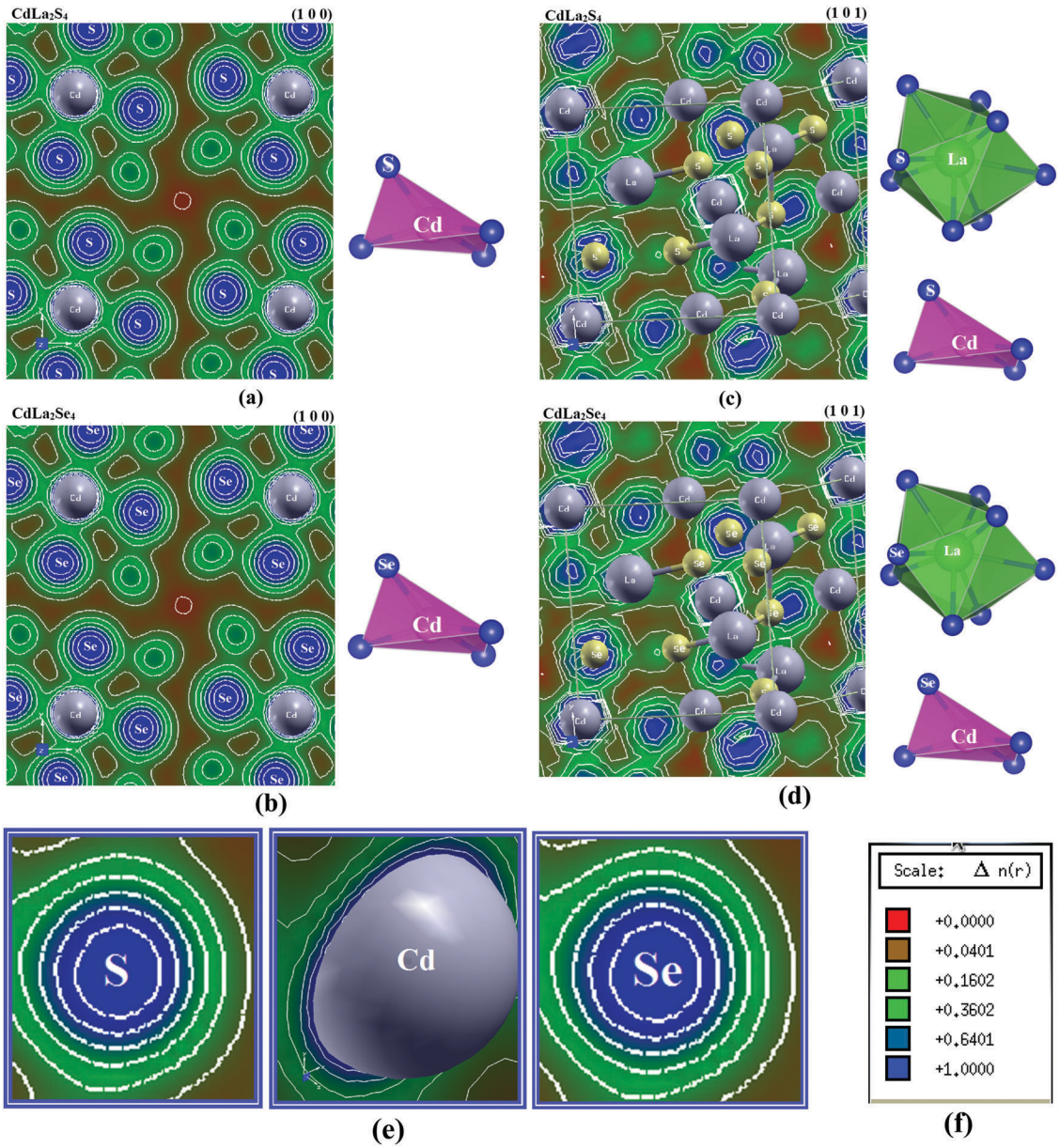

Fig. 5 The charge density distribution of $CdLa_2S_4$ in (100) plane; (b) the charge density distribution of $CdLa_2Se_4$ in (100) plane; (c) the charge density distribution of $CdLa_2S_4$ in (101) plane; (d) the charge density distribution of $CdLa_2Se_4$ in (101) plane; (e) shows an efficient charge transfer occurs towards Cd, S or Se atoms, as the Cd, S or Se atoms are surrounded by uniform spheres of charge density and the maximum charge accumulates around Cd, S or Se atoms as indicated by the blue color; (f) the thermoscale showing the blue color indicates the maximum charge intensity (1.0000).

Table 5 The calculated values of the ionic character

Bonds	P (%)
Cd–S	17.01
Cd–Se	16.34
La–S	31.34
La–Se	30.55

direct band gap nature for both compounds since the VBM and the CBM are situated at the Γ point of the BZ. The VB of $CdLa_2S_4$ ($CdLa_2Se_4$) is composed of S-3p (Se-4p), La-5p/4d and Cd-4p states, it is clear that the S-3p (Se-4p) states are responsible for constructing the VBM which could induce relatively localized photoholes; whereas La-5p/4d and Cd-4p states contribute little to the composition of the VBM. The CBM is mainly formed by Cd-5s states while La-6s/5p/4d, Cd-4p, and S-3s/3p (Se-5s/4p) states contribute little to the composition of the CBM. The angular momentum projected density of states reveal the hybridization between the states for instance Cd-5s and La-4d states strongly hybridized with S-3p (Se-4p) states, and meanwhile Cd-5s hybridized La-4d states. The hybridization may lead to the formation of covalent bonding depending on the degree of the hybridization, which is more favorable for the transport of the carriers than ionic bonding.[74] To support this statement and in order to reveal the chemical bonding properties of $CdLa_2S_4$ and $CdLa_2Se_4$, the electronic charge density is calculated in two crystallographic planes; (1 0 0) and (1 0 1) as shown in Fig. 5a–f. The charge localizes mainly between Cd and the neighboring S or Se atoms in the CdX_4 unit, and also between La and S or Se atoms in the LaX_8 unit indicating a partial ionic and strong covalent bonding. The strength of the interactions between the atoms is due to the degree of the hybridization and the electronegativity differences. According to the Pauling scale, the electro-negativity of Cd, La, S and Se are 1.69, 1.1, 2.58 and 2.55, respectively. To describe the character of the chemical bonding in $CdLa_2S_4$ and $CdLa_2Se_4$, the difference of the electronegativity ($X_A - X_B$) is crucial,[75] where X_A and X_B denotes the electronegativity of the A and B atoms in general. By increasing the ($X_A - X_B$) difference the ionic character (P) of the bonding increases. The percentage of P for the chemical bonding can be obtained using the expression:[75]

$$P\,(\%) = 16(X_A - X_B) + 3.5(X_A - X_B)^2 \qquad (3)$$

The calculated values of P are given in Table 5. It is clear that the Cd–S (Cd–Se) and La–S (La–Se) bonds are mostly covalent and partially ionic, see Table 5. The covalent bonding is more favorable for the transport of the carriers than ionic bonding.[74] Also, due to the electronegativity differences between the atoms, some valence electrons are transferred to S or Se atoms as it is clear that these atoms are surrounded by uniform blue spheres which indicate the maximum charge accumulation according to the thermoscale (Fig. 5f). The Cd–S, Cd–Se, La–S and La–Se units possess strong electron cloud overlap and prefer to attract holes and repel electrons, thus facilitating separation of the photogenerated e–h pairs. This in turn enhances the photocatalytic activity.[76]

4. Conclusions

The photocatalytic performances of two ternary semiconductor compounds namely $CdLa_2S_4$ and $CdLa_2Se_4$ have been investigated. *Ab initio* calculations from first- to second-principles methods were used to investigate the suitability of $CdLa_2S_4$ and $CdLa_2Se_4$ to be used as active photocatalysts under visible light illumination. The investigated compounds possess direct band gaps with absorption edges of about 579.3 nm and 670.1 nm, corresponding to the energy band gaps of 2.14 eV and 1.85 eV for $CdLa_2S_4$ and $CdLa_2Se_4$, respectively. The obtained energy band gap values are larger than the required value for splitting water under visible light illumination. The calculated E_{CB} and E_{VB} reveal that the investigated materials exhibit strong reducing powers for H_2 production and efficient photocatalysis for CO_2 photoreduction. $CdLa_2Se_4$ appears to be a more efficient photocatalyst for CO_2 photoreduction than $CdLa_2S_4$. While $CdLa_2S_4$ has a stronger reducing power for H_2 production than $CdLa_2Se_4$. A semiconductor with a more negative CB edge potential has a stronger reducing power for H_2 production from water. It can be clearly seen that the CB edge potential becomes more negative with increasing optical band gap and with substitution of Se by S. It has been found that $CdLa_2S_4$ and $CdLa_2Se_4$ possess high photogenerated carrier mobilities and favor enhancement of the photocatalytic performance. Furthermore, the obtained large mobility difference between the electrons (e^-) and holes (h^+) is useful for the separation of e^- and h^+, reduction of the e^- and h^+ recombination rate, and improvement of the photocatalytic activity. Thus non-centrosymmetric $CdLa_2S_4$ and $CdLa_2Se_4$ satisfied all the requirements to be efficient photocatalysts. This will greatly improve the search efficiency and greatly help experiments to save resources in the exploration of new photocatalysts with good photocatalytic performances.

Author contributions

A. H. Reshak, a professor with a PhD in physics and a PhD in materials engineering, performed the calculations, analyzed and discussed the results and wrote the manuscript.

Conflicts of interest

The author declares no competing financial interests.

Acknowledgements

The results were developed within the CENTEM project, reg. no. CZ.1.05/2.1.00/03.0088, cofunded by the ERDF as part of the Ministry of Education, Youth and Sports OP RDI programme and, in the follow-up sustainability stage, supported through CENTEM PLUS (LO1402) by financial means from the Ministry of Education, Youth and Sports under the National Sustainability Programme I. Computational resources were provided by MetaCentrum (LM2010005) and CERIT-SC (CZ.1.05/3.2.00/08.0144) infrastructures.

References

1 M. E. I. Zongwei, *Development of metal sulfide/Sdoped metal oxide photocatalysts for H_2 evolution from water under visible-light irradiation, PhD thesis,* Hokkaido University, 2013, DOI: 10.14943/doctoral.k11093, http://hdl.handle.net/2115/53925.
2 K. K. Banger, J. Cowen and A. F. Hepp, *Chem. Mater.*, 2001, **13**, 3827.
3 C. M. Joseph and C. S. Menon, *Semicond. Sci. Technol.*, 1996, **11**, 1668.
4 I. Tsuji, H. Kato and A. Kudo, *Angew. Chem., Int. Ed.*, 2005, **44**, 3565.
5 T. N. Meng, B. B. Chris and J. V. Jagadese, *J. Am. Chem. Soc.*, 2006, **128**, 7118.
6 X. Guangjian, G. Hongli, L. Peng and W. Guangming, *Appl. Mech. Mater.*, 2014, **556–562**, 362–365.
7 B. B. Kale, J. O. Baeg, K. J. Kong, S. J. Moon, L. K. Nikam and K. R. Patil, *J. Mater. Chem.*, 2011, **21**, 2624.
8 H. Miao, H. Li, Y. Cui, D. Tao, G. Wang and Y. Zhou, *Mater. Lett.*, 2014, **133**, 281.
9 Y. P. Yuan, S. W. Cao, L. S. Yin, L. Xu and C. Xue, *Int. J. Hydrogen Energy*, 2013, **38**, 7218.
10 L. Zhu and W.-C. Oh, *RSC Adv.*, 2015, **5**, 90321.
11 J. Hou, C. Yang, Z. Wang, S. Jiao and H. Zhu, *RSC Adv.*, 2012, **2**, 10330.
12 H. Liu, Z. Xu, Z. Zhang and D. Ao, *Appl. Catal., B*, 2016, **192**, 234.
13 L. Zhu and W.-C. Oh, *J. Korean Ceram. Soc.*, 2015, **52**, 173–179.
14 O. Y. Khyzhun, M. Piasecki, I. V. Kityk, I. Luzhnyi, A. O. Fedorchuk, P. M. Fochuk, S. I. Levkovets, M. V. Karpets and O. V. Parasyuk, *J. Solid State Chem.*, 2016, **242**, 193–198.
15 N. M. Denysyuk, V. L. Bekenev, M. V. Karpets, O. V. Parasyuk, S. P. Danylchuk and O. Y. Khyzhun, *J. Alloys Compd.*, 2013, **576**, 271–278.
16 O. Y. Khyzhun, V. L. Bekenev, N. M. Denysyuk, O. V. Parasyuk and A. O. Fedorchuk, *J. Alloys Compd.*, 2014, **582**, 802–809.
17 A. A. Lavrentyev, B. V. Gabrelian, V. T. Vu, P. N. Shkumat, G. L. Myronchuk, M. Khvyshchun, A. O. Fedorchuk, O. V. Parasyuk and O. Y. Khyzhun, *Opt. Mater.*, 2015, **42**, 351–360.
18 P. Blaha, K. Schwarz, G. K. H. Madsen, D. Kvasnicka and J. Luitz, *WIEN2k, An augmented plane wave plus local orbitals program for calculating crystal properties*, Vienna University of Technology, Austria, 2001.
19 J. P. Perdew, S. Burke and M. Ernzerhof, *Phys. Rev. Lett.*, 1996, **77**, 3865.
20 F. Tran and P. Blaha, *Phys. Rev. Lett.*, 2009, **102**, 226401.
21 G. K. H. Madsen and D. J. Singh, *Comput. Phys. Commun.*, 2006, **175**, 67–71.
22 P. B. Allen, in *Quantum Theory of Real Materials*, ed. J. R. Chelikowsky and S. G. Louie, Kluwer, Boston, 1996, pp. 219–250.
23 J. M. Ziman, *Electrons and Phonons*, Clarendon, Oxford, 2001.
24 C. M. Hurd, *The Hall Effect in Metals and Alloys*, Plenum, New York, 1972.
25 M. I. Kolinko, I. V. Kityk and A. S. Krochuk, *J. Phys. Chem. Solids*, 1992, **53**, 1315–1320.
26 G. E. Davydyuk, O. Y. Khyzhun, A. H. Reshak, H. Kamarudin, G. L. Myronchuk, S. P. Danylchuk, A. O. Fedorchuk, L. V. Piskach, M. Y. Mozolyuk and O. V. Parasyuk, *Phys. Chem. Chem. Phys.*, 2013, **15**, 6965.
27 A. H. Reshak, Y. M. Kogut, A. O. Fedorchuk, O. V. Zamuruyeva, G. L. Myronchuk, O. V. Parasyuk, H. Kamarudin, S. Auluck, K. L. Plucinskig and J. Bila, *Phys. Chem. Chem. Phys.*, 2013, **15**, 18979.
28 V. V. Atuchin, T. A. Gavrilova, J.-C. Grivel and V. G. Kesler, *Surf. Sci.*, 2008, **602**, 3095–3099.
29 V. V. Atuchin, T. A. Gavrilova, J.-C. Grivel and V. G. Kesler, *J. Phys. D: Appl. Phys.*, 2009, **42**, 035305.
30 O. Y. Khyzhun, V. L. Bekenev, V. V. Atuchin, E. N. Galashov and V. N. Shlegel, *Mater. Chem. Phys.*, 2013, **140**, 558–595.
31 V. V. Atuchin, E. N. Galashov, O. Y. Khyzhun, V. L. Bekenev, L. D. Pokrovsky, Y. A. Borovlev and V. N. Zhdankov, *J. Solid State Chem.*, 2016, **236**, 24–31.
32 K. Nouneh, A. H. Reshak, S. Auluck, I. V. Kityk, R. Viennois, S. Benet and S. Charar, *J. Alloys Compd.*, 2007, **437**, 39–46.
33 A. H. Reshak, K. Nouneh, I. V. Kityk, J. Bila, S. Auluck, H. Kamarudin and Z. Sekkat, *Int. J. Electrochem. Sci.*, 2014, **9**, 955–974.
34 H. Huang, Y. He, X. Li, M. Li, C. Zeng, F. Dong, X. Du, T. Zhangd and Y. Zhang, *J. Mater. Chem. A*, 2015, **3**, 24547–24556.
35 H. Huang, Y. He, Z. Lin, L. Kang and Y. Zhang, *J. Phys. Chem. C*, 2013, **117**, 22986–22994.
36 J. Zhang, W. Yu, J. Liu and B. Liud, *Appl. Surf. Sci.*, 2015, **358**, 457–462.
37 X. Li, J. Zhao and J. Yang, *Sci. Rep.*, 2013, **3**, 1858.
38 D. W. Hwang, J. S. Lee, W. Li and S. H. Oh, *J. Phys. Chem. B*, 2003, **107**, 4963–4970.
39 H. Huang, X. Li, J. Wang, F. Dong, P. K. Chu, T. Zhang and Y. Zhang, *ACS Catal.*, 2015, **5**, 4094–4103.
40 H. Huang, X. Han, X. Li, S. Wang, P. K. Chu and Y. Zhang, *ACS Appl. Mater. Interfaces*, 2015, **7**, 482–492.
41 C. Liu, Y. Zhang, F. Dong, A. H. Reshak, L. Ye, N. Pinna, C. Zeng, T. Zhang and H. Huang, *Appl. Catal., B*, 2017, **203**, 465–474; H. Huang, S. Tu, C. Zeng, T. Zhang, A. H. Reshak and Y. Zhang, *Angew. Chem., Int. Ed.*, 2017, **56**, 11860–11864.
42 A. H. Reshak, *J. Catal.*, 2017, **352**, 142–154; A. H. Reshak, *Phys. Chem. Chem. Phys.*, 2017, **19**, 24915; A. H. Reshak, *Appl. Catal., B*, 2018, **221**, 17–26; A. H. Reshak, *Appl. Catal., B*, 2018, **225**, 273–283; A. H. Reshak, *J. Alloys Compd.*, 2018, **741**, 1258–1268.
43 A. H. Reshak, *J. Catal.*, 2017, **351**, 119–129.
44 A. H. Reshak and S. Auluck, *J. Catal.*, 2017, **351**, 1–9.
45 https://materialsproject.org/materials/mp-36395/.
46 https://materialsproject.org/materials/mp-36733/.
47 P. E. Blöchl, O. Jepsen and O. K. Andersen, *Phys. Rev. B: Condens. Matter Mater. Phys.*, 1994, **49**, 16223.
48 H. Yan, X. Wang, M. Yao and X. Yao, *Prog. Nat. Sci.: Mater. Int.*, 2013, **23**, 402–407.
49 P. Zhou, J. H. Wu, W. L. Yu, G. H. Zhao, G. J. Fang and S. W. Cao, *Appl. Surf. Sci.*, 2014, **319**, 167–172.
50 T. Goldacker, V. Abetz, R. Stadler, I. Erukhimovich and L. Leibler, *Nature*, 1999, **398**, 137.

51 M. Stock and S. Dunn, *J. Phys. Chem. C*, 2012, **116**, 20854.
52 Y. Cui, J. Briscoe and S. Dunn, *Chem. Mater.*, 2013, **25**, 4215.
53 S. V. Kalinin and D. A. Bonnell, *Nanoscale Phenomena in Ferroelectric Thin Films*, Kluwer Academic Publications, Dordrecht, The Netherlands, 2004, pp. 182–216.
54 S. Dunn, P. M. Jones and D. E. Gallardo, *J. Am. Chem. Soc.*, 2007, **129**, 8724.
55 (*a*) Y. Inoue, K. Sate, K. Sato and H. Miyama, *J. Phys. Chem.*, 1986, **90**, 2809; (*b*) L. Li, P. A. Salvador and G. S. Rohrer, *Nanoscale*, 2014, **6**, 24; (*c*) M. E. Lines and A. M. Glass, *Principles and Applications of Ferroelectrics and Related Materials*, Clarendon Press, Oxford, UK, 2001.
56 M. T. Buelow and A. J. Gellman, *J. Am. Chem. Soc.*, 2001, **123**, 1440.
57 P. J. Zhou, G. Yu and M. Jaroniec, *Adv. Mater.*, 2014, **26**, 4920–4935.
58 Q. Li, H. Meng, P. Zhou, Y. Q. Zheng, J. Wang, J. G. Yu and J. R. Gong, *ACS Catal.*, 2013, **3**, 882–889.
59 X. Chang, T. Wang and J. Gong, *Energy Environ. Sci.*, 2016, **9**, 2177–2196.
60 H. Huang, Y. He, X. Li, M. Li, C. Zeng, F. Dong, X. Du, T. Zhangd and Y. Zhang, *J. Mater. Chem. A*, 2015, **3**, 24547–24556.
61 H. Huang, Y. He, Z. Lin, L. Kang and Y. Zhang, *J. Phys. Chem. C*, 2013, **117**, 22986–22994.
62 J. M. Carlsson, B. Hellsing, H. S. Domingos and P. D. Bristowe, *Phys. Rev. B: Condens. Matter Mater. Phys.*, 2002, **65**, 205122.
63 P. Dufek, P. Blaha and K. Schwarz, *Phys. Rev. B: Condens. Matter Mater. Phys.*, 1994, **50**, 7279.
64 A. H. Reshak, *RSC Adv.*, 2015, **5**, 22044–22052; A. H. Reshak, *RSC Adv.*, 2015, **5**, 33632–33638.
65 A. H. Reshak, H. Huang, H. Kamarudin and S. Auluck, *J. Appl. Phys.*, 2015, **117**, 085703.
66 A. H. Reshak, *Sci. Rep.*, 2017, **7**, 46415.
67 J. W. Tang and J. H. Ye, *Chem. Phys. Lett.*, 2005, **410**, 104–107.
68 T. L. Bahers, M. R. Rat and P. Sautet, *J. Phys. Chem. C*, 2014, **118**, 5997–6008.
69 J. Sato, H. Kobayashi and Y. Inoue, *J. Phys. Chem. B*, 2003, **107**, 7970–7975.
70 H. J. Zhang, L. Liu and Z. Zhou, *Phys. Chem. Chem. Phys.*, 2012, **14**, 1286–1292.
71 J. F. Zhang, P. Zhou, J. J. Liu and J. G. Yu, *Phys. Chem. Chem. Phys.*, 2014, **16**, 20382–20386.
72 J. Zhang, W. Yu., J. Liu and B. Liu, *Appl. Surf. Sci.*, 2015, **358**, 457–462.
73 J. Yang, P. Jiang, M. Yue, D. Yang, R. Cong, W. Gao and T. Yang, *J. Catal.*, 2017, **345**, 236–244.
74 F. Wu, H. Z. Song, J. F. Jia and X. Hu, *Prog. Nat. Sci.: Mater. Int.*, 2013, **23**, 408–412.
75 Schlusseltechnologien Key Technologies, vol. 11, ISBN 978-3-89336-559-3, 41st IFF Spring school, 2010, pp. A1–A18.
76 X. Fan, L. Zang, M. Zhang, H. Qiu, Z. Wang, J. Yin, H. Jia, S. Pan and C. Wang, *Chem. Mater.*, 2014, **26**, 3169–3174.